Optical properties of Al, Fe, Ti, Ta, W, and Mo at submillimeter wavelengths

Mark A. Ordal, Robert J. Bell, Ralph W. Alexander, Jr., Lawrence A. Newquist, and Marvin R. Querry

Measurements of the optical constants of metals at submillimeter wavelengths are sparse. We have used a nonresonant cavity to measure, at room temperature, the angle averaged absorptance spectra $P(\omega)$ of aluminum, molybdenum, tantalum, titanium, tungsten, and iron in the 30–300-cm^{-1} wavenumber region. The real part of the normalized surface impedance spectrum, $z(\omega) = r(\omega) + ix(\omega)$, was determined from $P(\omega)$. Measurements were also made on iron from 400 to 4000 cm^{-1} using standard reflectance techniques. The $r(\omega)$ spectrum was combined with previous measurements by others at higher frequencies and Kramers-Kronig analyses of the resultant combined $r(\omega)$ spectra provided $\varepsilon(\omega) = \varepsilon_1(\omega) + i\varepsilon_2(\omega)$ and $N(\omega) = n(\omega) + ik(\omega)$.

I. Introduction

The extremely high reflectivity of metals at submillimeter wavelengths generally precludes direct measurement of the reflectance or absorptance as is customary at shorter wavelengths. As a result, most of the measurements for metals have been made at wavelengths shorter than 5 or 10 μm; see Ref. 1–3, for example. Sievers and co-workers have pioneered measurements in the far infrared using two methods. They have measured the transmission of either nonresonant cavities[4,5] or plane-parallel waveguides[6] from which they could derive the real part of the normalized surface resistance. Their measurements were made at liquid helium temperatures.

We have recently reported measurements at room temperature for gold, nickel, and lead using a nonresonant cavity.[7] An improved method was used to calculate $r(\omega)$, the real part of the normalized surface impedance $z(\omega) = r(\omega) + ix(\omega)$ from 30 to 300 cm^{-1} from the measured transmission of the nonresonant cavity. We then used optical constants from the literature to calculate $r(\omega)$ at shorter wavelengths. The resulting $r(\omega)$ spectrum was Kramers-Kronig analyzed to obtain $x(\omega)$. By thus combining our far-infrared measurements with the literature for shorter wavelengths, we obtain the real and imaginary parts of the normalized surface impedance [or, equivalently, the real and imaginary parts of the dielectric function $\varepsilon(\omega) = \varepsilon_1(\omega) + i\varepsilon_2(\omega)$ or the real and imaginary parts of the refractive index $N(\omega) = n(\omega) + ik(\omega)$].[8]

A Perkin-Elmer model 580 spectrophotometer was used to measure the reflectance of the iron samples from 400 to 4000 cm^{-1} using a standard reflectance attachment. A Varian model 2300 was used for the 4000–50,000-cm^{-1} range.[3] An aluminum mirror, corrected for absolute reflectance, was used as a standard.

This paper extends three previous papers[3,7,9] (which summarized data available in the literature for a number of metals and reported Drude model fits to these data) by providing long-wavelength data for additional metals.

II. Experiment

A nonresonant cavity has no preferred standing wave modes and hence its dimensions must be large compared to all wavelengths of interest. Our cavity is cylindrical with plane end caps. The cylinder axis makes an angle of 4° with the plane of the end caps. One end plate was removable and was made either of the reference metal or the sample metal. The body and other end plate are made of the reference metal (aluminum in our case). Radiation enters through a small input hole and exits through another small hole. The transmission spectrum with the sample metal end plate, $I_s(\omega)$, and the transmission spectrum with the reference end plate, $I_r(\omega)$, were measured. Pinkerton and Sievers showed that[4]

Marvin Querry is with University of Missouri-Kansas City, Physics Department, Kansas City, Missouri 64110; the other authors are with University of Missouri-Rolla, Physics Department, Rolla, Missouri 65401.

Received 5 October 1987.
0003-6935/88/061203-07$02.00/0.

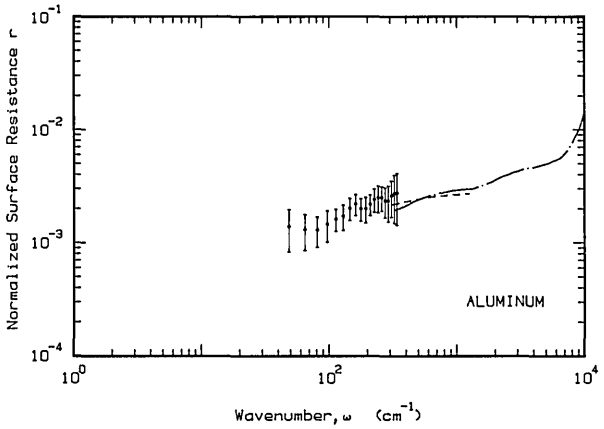

Fig. 1. Normalized surface impedance of aluminum. Dots with error bars were measured with a nonresonant cavity. The dash–dot line is from Shiles *et al.* (tabulated in Ref. 2) and the dashed line is from Bennett and Bennett.[11]

$$\frac{I_s(\omega)}{I_r(\omega)} - \frac{[2S_1 + (S_2 + S_3)P_r(\omega)] + S_4 P_r(\omega)}{[2S_1 + (S_2 + S_3)P_r(\omega)] + S_4 P_s(\omega)} = 0, \quad (1)$$

where $S_1 \equiv$ cross-sectional area of an input or output hole,

$S_2 \equiv$ area of the cavity sidewalls (excluding input and output holes),

$S_3 \equiv$ area of the bottom plate (which on our cavity is not normally removable),

$S_4 \equiv$ area of the removable top plate,

$P_r(\omega) \equiv$ angle averaged absorptance of the reference metal,

$P_s(\omega) \equiv$ angle averaged absorptance of the sample metal,

$I_s(\omega) \equiv$ intensity at frequency ω measured at the output hole of the cavity when the top plate of area S_4 is made of the sample metal, and

$I_r(\omega) \equiv$ intensity at frequency ω measured at the output hole of the cavity consists entirely of the reference metal.

For $P_s(\omega)$ and $P_r(\omega)$ we used the exact expression derived by Ordal *et al.*,[7]

$$P(\omega) \equiv 4r\left(\left[1 + \frac{1}{r^2(1+\xi^2)}\right] - \left[r + \frac{1}{r^3(1+\xi^2)}\right] \times \ln[1 + 2r + r^2(1+\xi^2)] + r\ln[r^2(1+\xi^2)] + \frac{(1-\xi^2)}{\xi}\left\{r\tan^{-1}\left[\frac{\xi}{1 + r(1+\xi^2)}\right] + \frac{1}{r^3(1+\xi^2)^2}\tan^{-1}\left(\frac{r\xi}{1+r}\right)\right\}\right). \quad (2)$$

As the optical constants for the sample are not known, and we have only one measurement [namely, the intensity ratio $I_s(\omega)/I_r(\omega)$], we made the approximation $\xi = 1$ in Eq. (2) when calculating P_s, leaving one unknown, $r_s(\omega)$ for the sample metal. This approximation is equivalent to setting the complex refractive index $N = n + ik = n(1 + i)$ for the sample metal. Note that one can use the approximation $\xi = 1$ as long as $1/\sqrt{(\varepsilon_1^2 + \varepsilon_2^2)} \ll 1$, even if $\xi \gg 1$. For $P_r(\omega)$, we used values of n and k for aluminum which had been measured in our laboratory. The values for aluminum were obtained using the measurements of Brandli and Sievers on gold foil and our measurements on Ni foil. This calibration procedure is described in detail in a previous paper.[7] Note that, after calculating $P_r(\omega)$ and $P_s(\omega)$ in this manner and inserting them into Eq. (1), we are left with an equation in one unknown, $r_s(\omega)$. Standard routines were used to find r_s.[10]

Because a single cavity with one changeable end plate was used, the cavity body and one end plate were identical for the sample and reference measurement. The samples (which were thin sheets or foils) were epoxied to a plate of 0.95-cm (0.375-in.) aluminum alloy before being mounted as the cavity end plate. The cavity and samples were polished with 1-μm diamond abrasive.

III. Results

A. Aluminum

The normalized surface resistance for aluminum obtained from the nonresonant cavity measurements is plotted in Fig. 1. The measurements of Shiles *et al.* (tabulated in Ref. 2) were used to calculate the normalized surface impedance from 320 to 7×10^6 cm^{-1}. A

Table I. Optical Constants of Aluminum

ω	n	k	$-\varepsilon_1$	ε_2	R
50	436.98909	485.19932	4445.8912	42405.361	0.995909
65	374.73526	431.44791	4572.0782	32335.749	0.995421
80	329.97183	393.77470	4617.7106	25986.911	0.995012
100	286.08777	357.47647	4594.3214	20453.929	0.994556
125	245.00980	324.59867	4533.4496	15905.971	0.994092
150	213.38844	299.72607	4430.1094	12791.616	0.993715
175	188.04844	279.77106	4290.9634	10522.102	0.993402
200	167.07810	263.04366	4127.6872	8789.7669	0.993141
225	149.32871	248.55977	3948.2895	7423.4221	0.992921
250	134.05166	235.70537	3758.7173	6319.3391	0.992734
300	108.95823	213.37170	3365.5586	4649.7203	0.992436
350	88.918176	192.23917	2904.9455	3418.7112	0.992103
400	76.681189	174.09538	2442.9198	2669.9682	0.991560
450	68.262241	159.23227	2069.5183	2173.9103	0.990944
500	61.871514	148.17314	1812.7196	1833.5393	0.990448
600	50.744867	131.07397	1460.5344	1330.2663	0.989778
700	42.226361	117.86671	1210.9495	995.41644	0.989283
800	35.492290	107.26425	1024.5918	761.41079	0.988941
900	30.167884	98.172167	872.76732	592.32931	0.988626
1000	25.832564	90.720430	756.28751	468.70826	0.988455
1250	17.708575	75.320562	535.95934	266.76396	0.988240
1500	13.385937	63.967532	391.26618	171.25308	0.987544
1750	10.625810	55.544522	297.22861	118.04110	0.986802
2000	8.8866481	49.131664	233.49479	873.23162	0.985847
2250	7.6669569	44.210650	189.57994	677.92230	0.984890
2500	6.5579910	40.184716	157.18041	527.06201	0.984310
2750	5.7888000	36.878956	132.65472	426.96980	0.983533
3000	5.0466806	34.058286	113.44979	343.76258	0.983129
3250	4.5104289	31.653186	981.58020	285.53889	0.982523
3500	4.0097886	29.575977	858.66002	237.18683	0.982175
3750	3.5693590	27.735962	756.54327	197.99921	0.981931
4000	3.1815630	26.073820	669.72172	165.91100	0.981750
4250	2.8842412	24.591905	596.44294	141.85797	0.981387
4500	2.6179915	23.257800	534.07140	121.77745	0.981098
4750	2.4038118	22.062867	480.99179	106.06996	0.980706
5000	2.1962737	20.969371	434.89089	92.108954	0.980475
5500	1.8892471	19.041604	359.01343	71.948588	0.979627
6000	1.6474236	17.430945	301.12384	57.432299	0.978801
6500	1.4501184	16.005291	254.06649	46.419134	0.977875
7000	1.3374754	14.766043	216.24717	39.498437	0.976063
7500	1.2712686	13.676589	185.43296	34.773235	0.973544
8000	1.2324984	12.721123	160.30791	31.357528	0.970446
8500	1.2366448	11.880035	139.60594	29.382766	0.966151
9000	1.2211025	11.108164	121.90021	27.128411	0.961937
9500	1.2553502	10.361271	105.78004	26.014047	0.955343
10000	1.3789601	9.6826848	91.852854	26.704071	0.944516
11000	2.0063894	8.4485537	67.352461	33.902178	0.900200
12000	2.7846191	8.3634734	62.193584	46.578175	0.867826
13000	2.6528613	8.7156916	68.925607	46.243043	0.881180
14000	2.0208103	8.5523233	69.058560	34.565246	0.901744
15000	1.6232262	8.0797904	62.648150	26.230654	0.910026

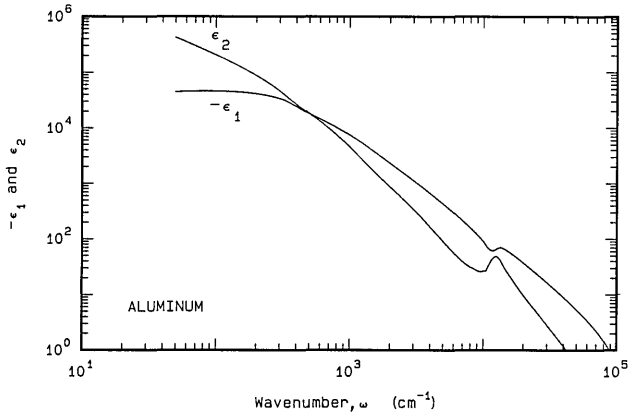

Fig. 2. ε_1 and ε_2 for aluminum derived from the Kramers-Kronig analysis as described in the text.

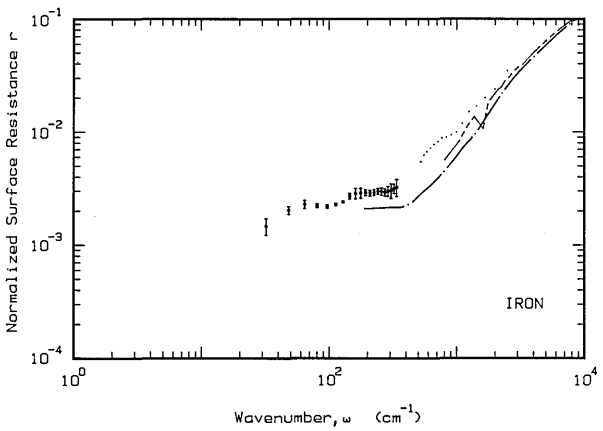

Fig. 3. Normalized surface impedance of iron. Dots with error bars were measured with a nonresonant cavity. The dash–dot line is from our reflectance measurements. The dotted line is from the measurements of Bolotin *et al.* and the short–long dash line is from the measurements of Weaver (both tabulated in Ref. 2).

Drude model with $\omega_\tau = 408\ \text{cm}^{-1}$ and $\omega_p = 92{,}700\ \text{cm}^{-1}$ was used for a low-frequency wing correction. The Drude model low-frequency calculations, the nonresonant cavity measurements, and the Shiles *et al.* measurements were combined and then the entire data set was Kramers-Kronig analyzed to obtain χ, the imaginary part of the normalized surface impedance. From r and χ the real imaginary parts of the dielectric function, ε_1 and ε_2, and the real and imaginary parts of the complex refractive index n and k were calculated. These are displayed in Table I, along with the calculated reflectance R. Figure 2 shows a plot of ε_1 and ε_2.

In a previous paper (Ref. 3), we fit the above data without the nonresonant cavity datum to a Drude model with $\omega_p = 119{,}000\ \text{cm}^{-1}$ and $\omega_\tau = 660\ \text{cm}^{-1}$. The surface resistance measured with the nonresonant cavity is better fit with $\omega_p = 95{,}400\ \text{cm}^{-1}$ and $\omega_\tau = 424\ \text{cm}^{-1}$.

B. Iron

The normalized surface resistance of iron mesured using the nonresonant cavity is plotted in Fig. 3. To

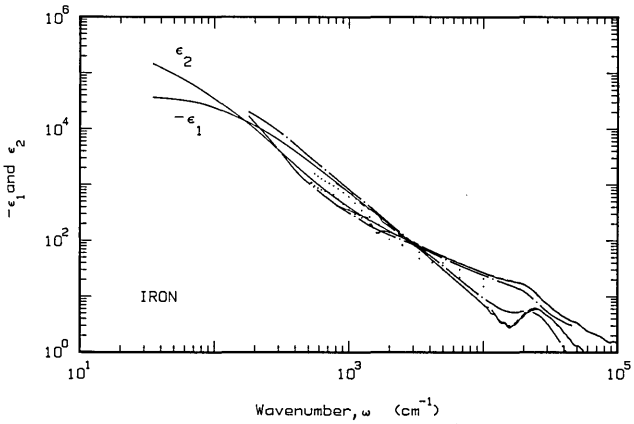

Fig. 4. ε_1 and ε_2 for iron. The solid curve is from the Kramers-Kronig analysis as described in the text. The dash–dot line is from Weaver *et al.* (tabulated in Ref. 2). The dotted line represents the results of Bolotin *et al.* (tabulated in Ref. 2).

Table II. Optical Constants of Iron

ω	n	k	$-\varepsilon_1$	ε_2	R
35	238.51940	305.98052	36732.576	145964.58	0.993681
50	183.41621	260.36949	34150.764	95511.971	0.992793
65	147.11263	230.22637	31362.058	67738.412	0.992148
80	120.39992	207.32665	28488.201	49924.224	0.991657
100	95.357710	181.94710	24011.654	34700.117	0.991002
125	75.191427	158.19090	19370.609	23789.199	0.990244
150	61.295883	140.34826	15940.449	17205.541	0.989601
175	51.169978	126.39007	13356.084	12934.754	0.989052
200	43.260218	115.07592	11371.020	9956.4184	0.988617
225	36.866495	105.45507	9761.6343	7775.5179	0.988254
250	31.895957	97.090004	8409.1168	6193.5571	0.987859
300	24.861494	83.533158	6359.6947	4153.5182	0.986995
350	20.259827	73.149608	4940.4046	2963.9968	0.986035
400	17.093309	65.004217	3933.3670	2222.2744	0.984983
450	14.820484	58.469983	3199.0922	1733.1069	0.983843
500	13.131270	53.124410	2649.7727	1395.1820	0.982618
600	10.825531	44.921725	1900.7693	972.60302	0.979932
700	9.3532527	38.936666	1428.5806	728.36895	0.976952
800	8.3467645	34.384013	1112.5918	573.99051	0.973703
900	7.6216326	30.807425	891.00812	469.60574	0.970211
1000	7.0686579	27.901743	728.54132	394.45575	0.966484
1250	6.1662033	22.672232	476.00804	279.60318	0.956375
1500	5.6202947	19.159671	335.50527	215.36599	0.945291
1750	5.2507160	16.634437	249.13446	174.68540	0.933488
2000	4.9822242	14.731832	192.20431	146.79458	0.921172
2250	4.7769777	13.247145	152.66734	126.56263	0.908513
2500	4.6139960	12.056655	124.07398	111.25872	0.895658
2750	4.4807297	11.081212	102.71632	99.303831	0.882728
3000	4.3691978	10.267835	86.338543	89.724403	0.869826
3250	4.2740535	9.5797246	73.503589	81.888511	0.857039
3500	4.1915574	8.9905172	63.260247	75.368537	0.844443
3750	4.1189946	8.4808227	54.958237	69.864925	0.832098
4000	4.0543264	8.0360513	48.140558	65.161549	0.820056
4250	3.9959802	7.6450020	42.478198	61.098554	0.808360
4500	3.9427114	7.2989194	37.729251	57.555066	0.797041
4750	3.8935181	6.9908450	33.712430	54.437963	0.786125
5000	3.8475818	6.7151655	30.289563	51.674297	0.775627
5500	3.7628981	6.2434063	24.820721	46.986604	0.755915
6000	3.6845745	5.8553312	20.708815	43.148808	0.737893
6500	3.6099615	5.5306374	17.556128	39.930777	0.721452
7000	3.5376077	5.2542311	15.092276	37.174816	0.706403
7500	3.4671150	5.0146674	13.126002	34.772857	0.692509
8000	3.3989889	4.8032972	11.518539	32.652708	0.679513
8500	3.3344296	4.6138021	10.168749	30.768797	0.667177
9000	3.2750676	4.4419211	9.0045955	29.095184	0.655318
9500	3.2227697	4.2852453	7.9770831	27.620718	0.643845
10000	3.1837613	4.1442444	7.0384258	26.388570	0.632770
11000	3.0937414	3.8974446	5.6188386	24.115371	0.612663
12000	3.0342872	3.7486080	4.8451634	22.748707	0.599798
13000	2.9736330	3.5471579	3.7398358	21.095891	0.580766
14000	2.9443374	3.4648084	3.3357743	20.403130	0.572707
15000	2.8735043	3.3589960	3.0258269	19.304179	0.562747

combine these results with measurements at shorter wavelengths, the following procedure was used. The data of Bolotin *et al.* (tabulated in Ref. 2) and of Weaver *et al.* (also tabulated in Ref. 2) were used in the region from 1000 to 242,000 cm^{-1}. Our reflection mea-

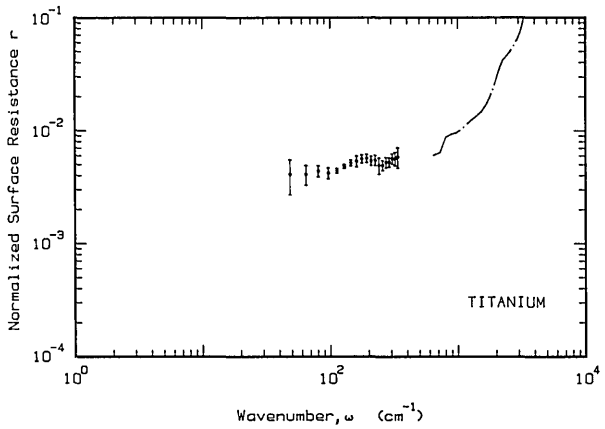

Fig. 5. Normalized surface impedance of titanium. The dots with error bars are from the nonresonant cavity measurements. The dash-dot line represents the measurements of Lynch, Olson, and Weaver (tabulated in Ref. 2).

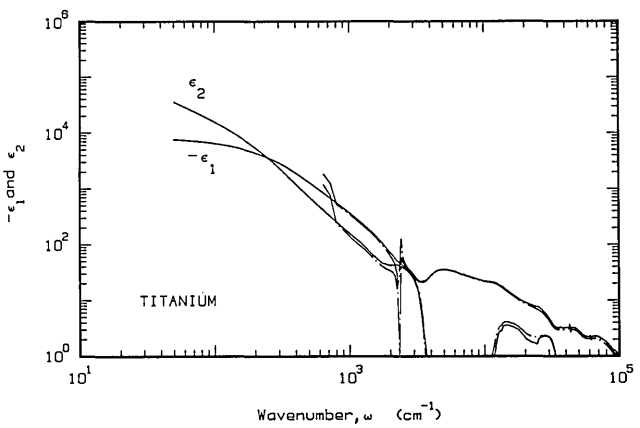

Fig. 6. ε_1 and ε_2 of titanium. The solid line is from the Kramers-Kronig analysis as described in the text. The dash-dot line is from the measurements of Lynch, Olson, and Weaver (tabulated in Ref. 2).

surements were used between 180 and 27,000 cm^{-1}. In regions of overlap, the various data sets were in reasonable agreement, and an average was taken. Beyond 242,000 cm^{-1} a high wing extrapolation corresponding to the reflectance falling off to one over the frequency to the fourth power was used. Below 100 cm^{-1}, a Drude model extrapolation was made using ω_τ = 156 cm^{-1} and ω_p = 29,500 cm^{-1}. These parameters were chosen to match smoothly to the nonresonant cavity results. The Kramers-Kronig analysis of this combined set of measurements resulted in the values of ε_1 and ε_2 shown in Fig. 4. Along with n and k and the calculated reflectance R, they are also tabulated in Table II.

Our previous Drude model fit[3] to the data without the nonresonant cavity results at long wavelengths gave ω_p = 33,000 cm^{-1} and ω_τ = 147 cm^{-1}. The nonresonant cavity data are not terribly well fit with a Drude model, but within the experimental error it can be fit with ω_p = 32,900 cm^{-1} and ω_τ = 213 cm^{-1}.

Table III. Optical Constants of Titanium

ω	n	k	$-\varepsilon_1$	ε_2	R
50	119.99544	148.43379	7633.6859	35622.757	0.986912
65	100.49717	131.88977	7295.2320	26509.097	0.985486
80	86.399911	120.07897	6954.0133	20749.624	0.984332
100	72.530316	108.42373	6495.0594	15728.015	0.983096
125	59.644857	97.484039	5945.6290	11628.843	0.981900
150	49.906684	88.904473	5413.3282	8873.8550	0.980980
175	42.303853	81.834224	4907.2242	6923.8059	0.980260
200	36.217641	75.809491	4435.3614	5491.2818	0.979688
225	31.260311	70.562709	4001.8888	4411.6244	0.979228
250	27.169229	65.925258	3607.9727	3582.2769	0.978855
300	20.880752	58.046709	2933.4146	2424.1179	0.978295
350	16.284041	51.475157	2384.5218	1676.4472	0.977908
400	13.299690	45.839465	1924.3748	1219.3013	0.976928
450	11.217047	41.326081	1582.0229	927.11318	0.975840
500	9.6744916	37.605191	1320.5546	727.62220	0.974676
600	7.5817542	31.846917	956.74316	482.91100	0.972123
700	6.2397504	27.621553	724.01572	344.70319	0.969389
800	5.2931800	24.380236	566.37815	258.09795	0.966605
900	4.5921948	21.789718	453.70355	200.12526	0.963703
1000	4.0715739	19.664351	370.10899	160.12972	0.960509
1250	3.2048691	15.799043	239.33857	101.26773	0.952039
1500	2.4841185	12.895769	160.13002	64.069237	0.944315
1750	2.1867059	10.536270	106.23131	46.079449	0.927812
2000	2.3660792	8.7896083	71.658884	41.593819	0.893164
2250	2.8327334	7.7291731	51.715738	43.789373	0.847764
2500	2.7313635	7.0189943	41.805934	38.342850	0.827100
2750	2.5809283	6.2578349	32.499306	32.302046	0.801404
3000	2.3943002	5.4204022	23.648086	25.956140	0.765850
3250	2.4004043	4.4865443	14.367139	21.539041	0.697032
3500	3.0649496	3.5829978	3.4439569	21.963415	0.582456
3750	3.8144105	3.0741948	−5.0990540	23.452481	0.532393
4000	4.3647610	3.1898829	−8.8757860	27.846153	0.551827
4250	4.6520327	3.3990496	−10.087870	31.624980	0.572217
4500	4.7418094	3.6030774	−9.5025890	34.170213	0.587225
4750	4.7311251	3.7288987	−8.4788590	35.283772	0.595202
5000	4.6752372	3.8164244	−7.2927480	35.685379	0.600180
5500	4.4682212	3.8823682	−4.8922180	34.694560	0.602597
6000	4.2746437	3.8609249	−3.3658370	33.008157	0.599833
6500	4.0126191	3.8077018	−1.6025190	30.557715	0.594940
7000	3.9419174	3.7122171	−1.7581570	29.266506	0.587267
7500	3.8097162	3.5906589	−1.6211060	27.358783	0.577006
8000	3.6981480	3.5123265	−1.3398610	25.978206	0.570096
8500	3.6009322	3.4342207	−1.1728410	24.732792	0.563026
9000	3.5179021	3.3609902	−1.0793800	23.647269	0.556208
9500	3.4440424	3.2989913	−0.9780839	22.723732	0.550281
10000	3.3957928	3.2418121	−1.0220630	22.017044	0.544683
11000	3.3065327	3.2405736	−0.4318412	21.430125	0.544673
12000	3.1079186	3.3007447	1.2357575	20.516891	0.552333
13000	2.8061078	3.2717366	2.8300195	18.361692	0.554422
14000	2.5658703	3.1836237	3.5517695	16.337531	0.550850
15000	2.3704320	3.0317254	3.5724114	14.372998	0.538628

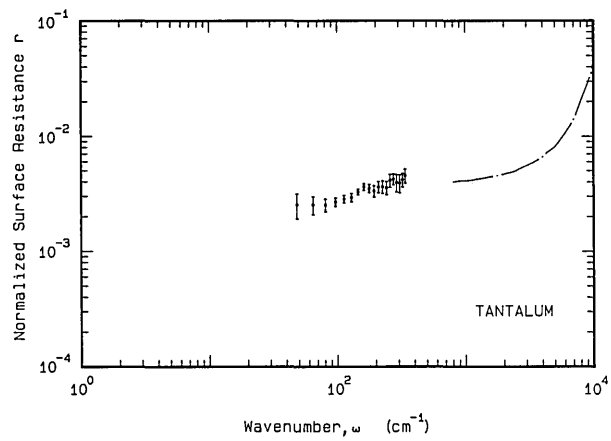

Fig. 7. Normalized surface impedance of tantalum. The dots with error bars are from the nonresonant cavity measurements. The dash-dot line represents the measurements of Weaver *et al.* (tabulated in Ref. 2).

Table IV. Optical Constants of Tantalum

ω	n	k	$-\varepsilon_1$	ε_2	R
80	184.49663	196.87085	4719.1248	72644.016	0.989914
100	164.07966	177.86128	4712.5008	58366.836	0.988854
125	145.58840	161.98150	5042.0233	47165.256	0.987798
150	131.25365	151.08524	5599.2281	39660.977	0.986978
175	119.43744	143.08774	6208.7985	34180.068	0.986342
200	109.23359	136.82885	6790.1559	29892.614	0.985848
225	100.17673	131.63028	7291.1522	26372.582	0.985462
250	92.016211	127.08528	7683.6846	23387.811	0.985160
300	77.867703	119.08288	8117.3521	18545.420	0.984732
350	66.138800	111.86857	8140.2353	14797.706	0.984458
400	56.428490	105.16669	7875.8590	11868.796	0.984280
450	48.392026	98.921392	7443.6535	9574.0132	0.984166
500	41.721911	93.122866	6931.1502	7770.5278	0.984101
600	31.493393	82.794230	5863.0508	5214.9424	0.984076
700	24.238520	73.949845	4881.0737	3584.8696	0.984120
800	19.058763	66.350003	4039.0864	2529.0980	0.984133
900	15.615760	59.926459	3347.3285	1871.5944	0.983848
1000	12.931507	54.673721	2821.9919	1414.0272	0.983751
1250	8.7691085	44.613332	1913.4521	782.43829	0.983183
1500	6.4122619	37.643719	1375.9325	482.76277	0.982575
1750	4.9008382	32.510917	1032.9415	318.66149	0.982045
2000	3.9020861	28.577040	801.42097	223.02015	0.981434
2250	3.1932058	25.461819	638.10767	162.60966	0.980818
2500	2.6799222	22.915456	517.93616	122.82328	0.980099
2750	2.3469537	20.845754	429.03725	97.848038	0.979939
3000	2.0587589	19.120563	361.35743	78.729256	0.978037
3250	1.8209204	17.640057	307.85584	64.242278	0.977176
3500	1.6348171	16.359682	264.96656	53.490174	0.976185
3750	1.4802727	15.240124	230.07017	45.119079	0.975165
4000	1.3499202	14.239580	200.94335	38.444593	0.974076
4250	1.2678805	13.363144	176.96610	33.885739	0.972395
4500	1.1923530	12.595572	157.22672	30.036736	0.970821
4750	1.1067824	11.896174	140.29399	26.332953	0.969668
5000	1.0326738	11.243595	125.35202	23.221933	0.968359
5500	0.9608260	10.114648	101.38292	19.436833	0.963794
6000	0.9019896	9.1771344	83.406210	16.555360	0.958925
6500	0.8564461	8.3686838	69.301368	14.334653	0.953379
7000	0.8354757	7.6548582	57.898834	12.790895	0.946069
7500	0.8414308	7.0171487	48.532371	11.808890	0.936051
8000	0.8740663	6.4776281	41.195673	11.323753	0.923111
8500	0.9012078	6.0121558	35.333842	10.836403	0.909337
9000	0.9253053	5.5894492	30.385753	10.343894	0.894096
9500	0.9603200	5.2167868	26.292650	10.019570	0.876318
10000	0.9821499	4.8873028	22.921110	9.6001281	0.858758
11000	1.0150307	4.2736932	17.234167	8.6758595	0.818134
12000	1.0730870	3.7362305	12.807903	8.0186007	0.764894
13000	1.1466787	3.2384897	9.1729431	7.4270145	0.696164
14000	1.2685432	2.7919609	6.1858440	7.0834463	0.607910
15000	1.4478379	2.3306224	3.3355663	6.7487268	0.493041

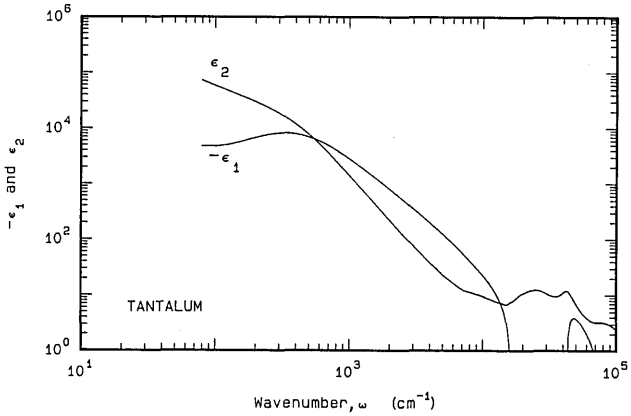

Fig. 8. ε_1 and ε_2 of tantalum from the Kramers-Kronig analysis as described in the text.

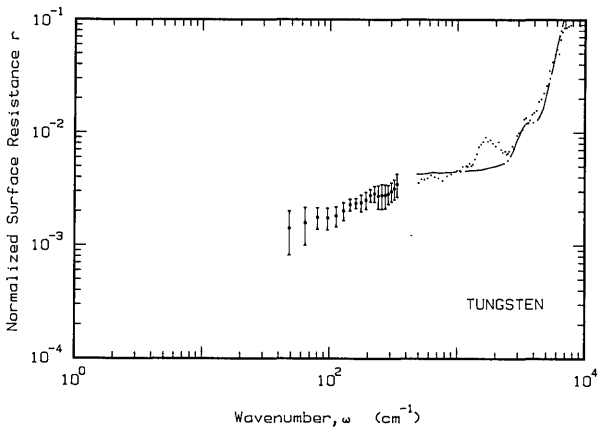

Fig. 9. Normalized surface impedance for tungsten. The dots with error bars are the nonresonant cavity measurements. The dash–dot line represents the results of Weaver, Lynch, and Olson (tabulated in Ref. 2). The dotted line is the results of Nomerovannaya *et al.*[12]

C. Titanium

Figure 5 shows the normalized surface impedance obtained from the nonresonant cavity. Again a Drude model fit was used to obtain a low-frequency wing for the Kramers-Kronig analysis. The Drude model parameters were $\omega_\tau = 372\ \text{cm}^{-1}$ and $\omega_p = 25{,}000\ \text{cm}^{-1}$. At shorter wavelengths, the measurements of Lynch *et al.* (tabulated in Ref. 2) were used (1290–24,000 cm^{-1}). The gap between our nonresonant cavity measurements and Lynch's was filled using a spline fit. Shown in Fig. 6 are ε_1 and ε_2. In Table III are the values of ε_1, ε_2, n, k, and the calculated reflectance.

Previously[3] we fit the short-wavelength data for titanium with a Drude model with $\omega_p = 20{,}300\ \text{cm}^{-1}$ and $\omega_\tau = 382\ \text{cm}^{-1}$. The nonresonant cavity data are very well fit by the Drude model, but with $\omega_p = 20{,}900\ \text{cm}^{-1}$ and $\omega_\tau = 243\ \text{cm}^{-1}$.

D. Tantalum

The normalized surface impedance of tantalum is shown in Fig. 7. To perform the Kramers-Kronig analysis, a Drude low-frequency wing was used with $\omega_\tau = 470\ \text{cm}^{-1}$ and $\omega_p = 50{,}000\ \text{cm}^{-1}$. The data of Weaver *et al.* (tabulated in Ref. 2) were used from 800 to 322,600 cm^{-1}. The gap between the nonresonant cavity measurements and those of Weaver was filled with a spline fit. After Kramers-Kronig analysis of this combined set of data, ε_1, ε_2, n, k, and R were calculated. These are tabulated in Table IV and ε_1 and ε_2 are plotted in Fig. 8.

The short-wavelength tantalum data cannot be satisfactorily fit with the Drude model. The nonresonant cavity data can just be fit within the experimental errors with $\omega_p = 66{,}200\ \text{cm}^{-1}$ and $\omega_\tau = 704\ \text{cm}^{-1}$ although the data do not appear to have the right shape.

E. Tungsten

Figure 9 shows the measured surface impedance for tungsten. A low-frequency Drude wing was generated using $\omega_\tau = 250\ \text{cm}^{-1}$ and $\omega_p = 50{,}000\ \text{cm}^{-1}$. The data of Weaver *et al.* (tabulated in Ref. 2) were used from 3700 to 32,000 cm^{-1}. The region between our far-infrared and Weaver's near-infrared data was filled using a spline fit to the ends of both data sets. After Kramers-Kronig analysis of this joint data set, the values of the dielectric function, refractive index, and reflectivity shown in Table V were calculated. Figure 10 shows ε_1 and ε_2.

Table V. Optical Constants of Tungsten

ω	n	k	$-\epsilon_1$	ϵ_2	R
50	242.14161	332.81796	52135.234	161178.15	0.994299
65	196.84283	294.94073	48242.936	116113.94	0.993758
80	163.02849	265.86909	44108.085	86688.476	0.993318
100	130.21900	234.03939	37817.448	60952.753	0.992765
125	103.53408	202.21197	30170.375	41871.663	0.992008
150	87.148396	177.92054	24060.874	31010.979	0.991158
175	76.505227	159.83902	19695.461	24457.041	0.990302
200	68.665703	146.58093	16770.990	20130.165	0.989572
225	61.731428	136.67195	14868.452	16873.909	0.989081
250	54.191208	128.08146	13468.174	13881.779	0.988856
300	44.209069	112.34062	10665.974	9932.9489	0.987941
350	37.127733	100.62038	8745.9914	7471.6129	0.987173
400	31.772550	91.217414	7311.1217	5796.4198	0.986472
450	27.599188	83.517367	6213.4354	4610.0231	0.985834
500	24.256111	77.087223	5354.0811	3739.6725	0.985255
600	19.231714	66.923752	4108.9298	2574.1169	0.984262
700	15.634532	59.208636	3261.2239	1851.3986	0.983466
800	12.935818	53.112521	2653.6045	1374.1078	0.982839
900	10.843912	48.146015	2200.4483	1044.1823	0.982356
1000	9.1935519	44.019189	1853.1676	809.38539	0.981988
1250	6.2868052	36.072044	1261.6684	453.55582	0.981431
1500	4.4961625	30.343034	900.48423	272.85443	0.981087
1750	3.3712766	26.005432	664.91701	175.34301	0.980608
2000	2.6672954	22.612178	504.19613	120.62672	0.979668
2250	2.2388765	19.898510	390.93813	89.100611	0.977966
2500	1.9949739	17.694770	309.12496	70.601208	0.975223
2750	1.8774806	15.887186	248.87776	59.655769	0.971191
3000	1.8505739	14.400460	203.94863	53.298233	0.965650
3250	1.9169200	13.261664	172.19714	50.843098	0.958414
3500	1.8748013	12.375593	149.64041	46.403556	0.953542
3750	1.6746349	11.554665	130.70589	38.699691	0.952379
4000	1.4507921	10.710594	112.61204	31.077692	0.951930
4250	1.2886548	9.8569158	95.498158	25.404325	0.949660
4500	1.2212030	9.0476312	80.368294	22.097989	0.943719
4750	1.1946455	8.2613235	66.822288	19.738707	0.934599
5000	1.2992808	7.5659499	55.555468	19.660587	0.916886
5500	1.5455798	6.4453363	39.153543	19.923564	0.871262
6000	1.8828191	5.4881071	26.574312	20.666226	0.804026
6500	2.2587782	4.7741297	17.690236	21.567400	0.729584
7000	3.0278249	4.3901355	10.105566	26.585123	0.658805
7500	3.1990778	4.4460869	9.5335904	28.446756	0.657852
8000	3.1960757	4.3367596	8.5925835	27.721224	0.648923
8500	3.1599449	4.1791582	7.4801119	26.411819	0.636480
9000	3.0821649	3.9693342	6.2558737	24.468285	0.619717
9500	3.0570934	3.7224010	4.5104492	22.759456	0.596640
10000	3.0826871	3.4208368	2.1991647	21.090740	0.565367
11000	3.2814572	3.0100921	-1.7073070	19.754977	0.520807
12000	3.5190631	2.7670600	-4.7271840	19.474918	0.498683
13000	3.7783360	2.6322954	-7.3468440	19.891393	0.492184
14000	3.9313491	2.7924078	-7.6579650	21.955860	0.510352
15000	3.8312601	2.9042727	-6.2437540	22.254049	0.517715

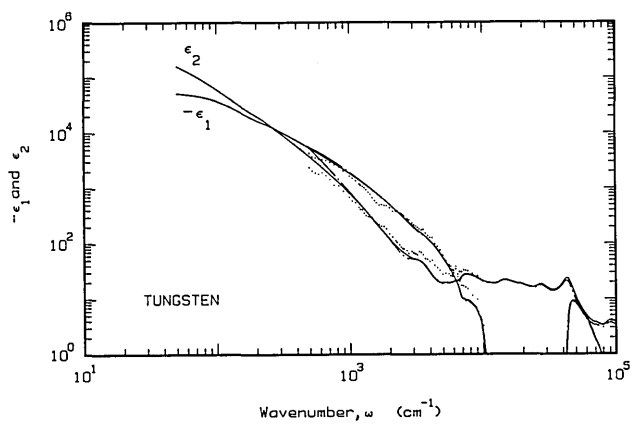

Fig. 10. ε_1 and ε_2 of tungsten. The solid line is from the Kramers-Kronig analysis described in the text. The dash–dot line is the data of Weaver, Lynch, and Olson (tabulated in Ref. 2). The dotted curve is the data of Nomerovannaya *et al.*[12]

The surface impedance measured using the nonresonant cavity is not well fit with a Drude model.

F. Molybdenum

The normalized surface impedance of molybdenum is plotted vs wavenumber in Fig. 11. For the Kramers-Kronig analysis, a low-frequency Drude wing with ω_τ = 412 cm^{-1} and ω_p = 60,200 cm^{-1} was matched to the nonresonant cavity measurements. The optical constants determined by Lynch and Hunter (tabulated in Ref. 1) were used from 800 to 1.6 × 10^6 cm^{-1}. As usual, a spline fit was used in the gap between these two sets of measurements. The dielectric function obtained from the Kramers-Kronig analysis is shown vs frequency in Fig. 12. Table VI contains the dielectric function, the complex refractive index, and the calculated reflectance as a function of wavenumber.

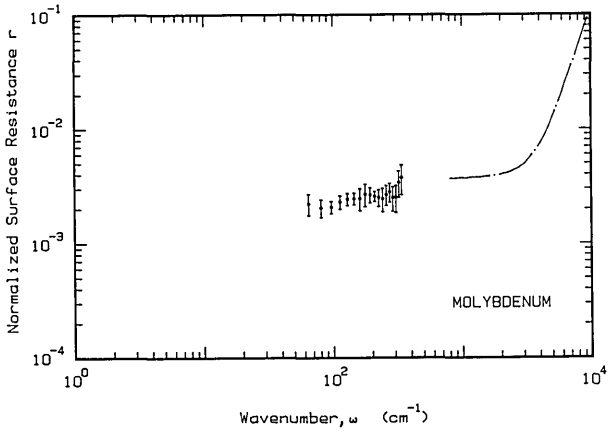

Fig. 11. Normalized surface impedance for molybdenum. The dots with error bars are the nonresonant cavity results. The dash–dot curve displays the results of Lynch and Hunter (tabulated in Ref. 2).

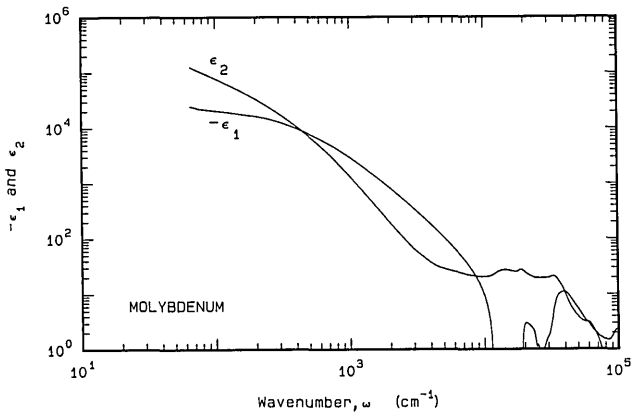

Fig. 12. ε_1 and ε_2 of molybdenum from the Kramers-Kronig analysis described in the text.

The surface impedance measured with the nonresonant cavity is well fit with a Drude model with ω_p = 58,600 cm^{-1} and ω_τ = 417 cm^{-1}. The parameters agree well with those of our previous fit[3] to the shorter wavelength measurements (ω_p = 60,200 cm^{-1} and ω_τ = 412 cm^{-1}).

This work was partially supported by the U.S. Army CRDEC contract DAAA-15-85-K-0004 (M. Milham and J. Embury).

Mark Ordal is currently at the North Dakota State University.

Table VI. Optical Constants of Molybdenum

ω	n	k	$-\epsilon_1$	ϵ_2	R
65	227.57460	276.18720	24489.170	125706.39	0.992917
80	200.43914	248.88501	21767.898	99772.593	0.992180
100	173.64793	224.74485	20356.642	78052.956	0.991426
125	148.54398	202.91175	19107.865	60282.639	0.990648
150	129.77236	186.39648	17902.784	48378.221	0.989988
175	114.94950	173.65334	16942.094	39922.730	0.989454
200	102.12640	163.32577	16245.505	33359.746	0.989051
225	91.330970	154.08616	15401.198	28145.676	0.988678
250	82.241906	145.83988	14505.539	23988.299	0.988334
300	67.891603	131.81545	12766.043	17898.324	0.987724
350	57.122067	120.35199	11221.672	13749.509	0.987209
400	48.760817	110.79000	9896.8064	10804.422	0.986777
450	42.092997	102.66741	8768.7765	8643.1578	0.986419
500	36.663706	95.659355	7806.4849	7014.4529	0.986124
600	28.406166	84.122793	6269.7341	4779.2120	0.985692
700	22.527740	75.010773	5119.1170	3379.6464	0.985419
800	17.948846	67.549462	4240.7687	2424.8698	0.985413
900	14.599652	61.094152	3519.3455	1783.9067	0.985312
1000	12.132436	55.822815	2968.9906	1354.5334	0.985243
1250	8.0417701	45.523100	2007.6825	732.17260	0.985067
1500	5.7374219	38.275608	1432.1042	439.20663	0.984806
1750	4.3080595	32.926140	1065.5713	283.69553	0.984508
2000	3.3460153	28.788898	817.60482	192.65619	0.984211
2250	2.7142480	25.500166	642.89134	138.42755	0.983650
2500	2.2903056	22.850789	516.91304	104.67058	0.982811
2750	1.9643186	20.649783	422.55498	81.125506	0.981946
3000	1.7296250	18.769452	349.30071	64.928225	0.980768
3250	1.6006395	17.177196	292.49402	54.988998	0.978787
3500	1.5147128	15.828837	248.25772	47.952285	0.976413
3750	1.4347181	14.654142	212.68547	42.049125	0.973994
4000	1.3719253	13.607095	183.27087	37.335836	0.971235
4250	1.3358240	12.667669	158.68541	33.843553	0.967797
4500	1.3246140	11.821314	137.98887	31.317357	0.963496
4750	1.3419643	11.064120	120.61389	29.695309	0.958031
5000	1.3787354	10.396535	106.18703	28.668141	0.951515
5500	1.4476138	9.2513402	83.491710	26.784735	0.936770
6000	1.5124883	8.2838453	66.334472	25.058437	0.919264
6500	1.6167352	7.4926629	53.526165	24.227304	0.897329
7000	1.7014062	6.7993804	43.336791	23.137016	0.872861
7500	1.7797564	6.1751066	34.964409	21.980371	0.844763
8000	1.9061057	5.6230394	27.985333	21.436215	0.809694
8500	2.0338468	5.1486289	22.371847	20.943045	0.772198
9000	2.1691522	4.7136001	17.512805	20.449032	0.731054
9500	2.3419619	4.3245235	13.216718	20.255738	0.686382
10000	2.5372515	3.9968299	9.5370042	20.281926	0.643729
11000	2.9807157	3.4956418	3.3348457	20.839029	0.575179
12000	3.4879914	3.2991627	-1.2816100	23.014903	0.550322
13000	3.7771262	3.4266289	-2.5248970	25.885619	0.562867
14000	3.8159832	3.5417088	-2.0180270	27.030203	0.572886
15000	3.7361860	3.5912220	-1.0622100	26.834947	0.576976

References

1. E. D. Palik, *Handbook of Optical Constants of Solids* (Academic, New York, 1985).
2. J. H. Weaver, C. Krafka, D. W. Lynch, and E. E. Koch, *Physics Data, Optical Properties of Metals, Part I: the Transition Metals* and *Physics Data, Optical Properties of Metals, Part II: the Noble Metals, Aluminum, Scandium, Yttrium, the Lanthanides, and the Actinides* (Fachinformationszentrum, 7514 Eggenatein-Leopoldshafen 2, Karlsruhe, F.R. Germany, 1981).
3. M. A. Ordal, R. J. Bell, R. W. Alexander, Jr., L. L. Long, and M. R. Querry, "Optical Properties of Fourteen Metals in the Infrared and Far Infrared: Al, Co, Cu, Au, Fe, Pb, Mo, Ni, Pd, Pt, Ag, Ti, V, and W," Appl. Opt. **24,** 4493 (1985).
4. F. E. Pinkerton and A. J. Sievers, "Quantitative FIR Absorptivity Measurements of Metals with Dual Nonresonant Cavities," Infrared Phys. **22,** 377 (1982).
5. F. E. Pinkerton, A. J. Sievers, M. B. Maple, and B. C. Sales, "Enhanced Far-Infrared Absorption in $CdPd_3$ and $YbCuSi_2$ Experiment," Phys. Rev. B **29,** 609 (1984).
6. G. Brandli and A. J. Sievers, "Absolute Measurement of the Far-Infrared Surface Resistance of Pb," Phys. Rev. B **5,** 3550 (1972).
7. M. A. Ordal, R. J. Bell, R. W. Alexander, Jr., L. L. Long, and M. R. Querry, "Optical Properties of Au, Ni, and Pb at Submillimeter Wavelengths," Appl. Opt. **26,** 744 (1987).
8. R. J. Bell, M. A. Ordal, and R. W. Alexander, Jr., "Equations Linking Different Sets of Optical Properties for Nonmagnetic Materials," Appl. Opt. **24,** 3680 (1985).
9. M. A. Ordal, L. L. Long, R. J. Bell, S. E. Bell, R. R. Bell, R. W. Alexander, Jr., and C. A. Ward, "Optical Properties of the Metals Al, Co, Cu, Au, Fe, Pb, Ni, Pd, Pt, Ag, Ti, and W in the Infrared and Far Infrared," Appl. Opt. **22,** 1099 (1983).
10. W. H. Press, B. P. Flannery, S. A. Teukolsky, and W. T. Vetterling, *Numerical Recipes: the Art of Scientific Computing* (Cambridge U.P., New York, 1986).
11. H. E. Bennett and J. M. Bennett, "Validity of the Drude Theory for Silver, Gold and Aluminum in the Infrared," in *Optical Properties and Electronic Structure of Metals and Alloys,* F. Abeles, Ed. (North-Holland, Amsterdam, 1966), p. 175.
12. L. V. Nomerovannaya, M. M. Kirillova, and M. M. Noskov, "Optical Properties of Tungsten Monocrystals," Sov. Phys. JETP **33,** 405 (1971).